Local structure investigation of Ga and Yb dopants in Co_{4}Sb_{12} skutterudites

Yanyun Hu, Ning Chen, J. P. Clancy, James R. Salvador, Chang-Yong Kim, Xiaoya Shi, Qiang Li, and Young-June Kim

Local structure investigation of Ga and Yb dopants in Co_4Sb_{12} skutterudites

Yanyun Hu,[1] Ning Chen,[2] J. P. Clancy,[1] James R. Salvador,[3]
Chang-Yong Kim,[2] Xiaoya Shi,[4] Qiang Li,[4] and Young-June Kim[1, *]

[1] *Department of Physics, University of Toronto, 60 St. George Street, Toronto, Ontario M5S 1A7, Canada*
[2] *Canadian Light Source, Saskatoon, Saskatchewan S7N 0X4, Canada*
[3] *Chemical and Materials Systems Lab, General Motors R& D Center, Warren, Michigan 48090, USA*
[4] *Condensed Matter Physics and Materials Science Department,*
Brookhaven National Laboratory, Upton, New York 11973, USA
(Dated: December 13, 2017)

We report comprehensive x-ray absorption spectroscopy studies at both Ga K-edge and Yb L_2-edge to elucidate the local structure of Ga and Yb dopants in $Yb_xGa_yCo_4Sb_{12}$. Our extended x-ray absorption fine structure (EXAFS) data confirm that Ga atoms occupy two crystallographic sites: one is the $24g$ site replacing Sb, and the other is the $2a$ site in the off-center void position. We find that the occupancy ratio of these two sites varies significantly as a function of the filling fraction of additional Yb, which exclusively occupies the $2a$ on-center site. At low concentrations of Yb, Ga_{24g} and Ga_{2a} dopants coexist and they form a charge-compensated compound defect proposed by Qiu et al. [Adv. Funct. Mater. 23, 3194 (2013)]. The Ga_{24g} occupancy increases gradually with increasing Yb concentration, and almost all Ga occupies the $24g$ site for the highest Yb concentration studied($x = 0.4$). In addition to the local structural evidence provided by our EXAFS data, we also present x-ray absorption near-edge structure (XANES) spectra, which show a small Ga K-edge energy shift as a function of Yb concentration consistent with the change from predominantly Ga_{2a} to Ga_{24g} states. Our result suggests that the increased solubility of Yb in Yb-Ga co-doped Co_4Sb_{12} skutterudites is due to the increased Ga_{24g} electron acceptor, and thus provides an important strategy to optimize the carrier concentration in partially filled skutterudites.

I. INTRODUCTION

The skutterudites with the chemical formula M_4X_{12} (M=Co, Rh or Ir; X=P, As or Sb) have attracted much attention as promising thermoelectric materials for moderate- and high-temperature energy harvesting[1–7]. These compounds crystallize into a body-centered-cubic structure (space group $Im\bar{3}$), in which a large void is created by 8 surrounding MX_6 octahedra. The voids can be filled with a variety of guest atoms, such as rare earth, alkaline earth and alkali metals, giving rise to extremely varied electronic and thermal properties[8–10]. The filler atom fraction can also be used to tune the carrier concentration and optimize electrical performance[11,12]. One of the reasons why filled skutterudites have very high thermoelectric efficiency (ZT) values is the reduced lattice thermal conductivity, κ_l, due to the structure of host network and guest filler atoms. It has been widely believed that the so-called 'rattling' vibration of the filler atoms reduces κ_l[13–17]. However, recent studies report that the suppressed κ_l is due to the quasi-harmonic interaction between the host lattice and the filler atoms[18–20]. Though the precise mechanism for how the guest atoms hinder heat propagation is under debate, it is very clear that the guest atom plays a significant role in determining both electrical and lattice properties. Extensive effort has been put into investigating thermoelectric properties when different filler atoms are used[4,21–28]. Another actively investigated research area is the effect of two or more dissimilar fillers[29–35].

While most discussions in filled skutterudites focus on the typical void site fillers such as rare-earth or alkaline-earth ions, it is important to note that group 13 elements such as Ga or In exhibit quite unique properties. Although earlier density functional theory studies predicted that such filling would be energetically unfavorable[26], a number of experimental studies reported that Ga/In can fill the voids in the Co_4Sb_{12} structure.[30,36–38] What is very intriguing is that these Ga- or In-doped materials show improved thermoelectric performance,[30,36–38] despite the small solubility of Ga/In in Co_4Sb_{12}[39,40]. To explain this surprising thermoelectric properties of Ga and In filled Co_4Sb_{12} skutterudite, a complex compound defect model has been proposed[41]. This model allows Ga impurity atoms replacing Sb atoms ($24g$ Wyckoff sites) within the Sb host network, in addition to the usual void-filling sites ($2a$ Wyckoff sites). Since Ga in the $24g$ site acts as an electron acceptor, unlike the $2a$ site Ga (electron donor), the charge is compensated and the materials can be treated as a nearly intrinsic semiconductor[41,42]. Such charge-compensated compound defects (CCCD) reduce lattice thermal conductivity, and allows facile incorporation of secondary filler atoms, such as Yb, which can be independently used to control the carrier concentration. Recent studies also suggest that the band structure modification due to the $24g$-site Ga enhances effective mass, which explains enhanced thermopower[43].

Previous electrical and thermal transport[44], microstructural and compositional variation studies[41,44,45] have reported results consistent with the CCCD picture. In recent high resolution scanning transmission electron microscopy (STEM) studies, structural distortion and intensity variation was interpreted as a particular type of CCCD due to Ga occupying both $2a$ and $24g$ sites in

$Yb_{0.26}Ga_{0.2}Co_4Sb_{12}$[43]. However, direct structural confirmation of Ga replacing Sb in 24g-site is still lacking, partly due to the experimental difficulty. Conventional x-ray or neutron diffraction is not very sensitive to the small amount (about 1 %) of dopant atoms in these materials. In addition, the random distribution of Ga atoms between void filling and Sb substitutional sites makes it difficult to carry out structural refinements, since diffraction averages over the entire sample.

Extended x-ray absorption fine structure (EXAFS) is a powerful probe to address these issues in an element-specific manner. The interference patterns in the EXAFS spectra can be used to obtain quantitative information about the local structure near an absorbing atom. During the past three decades, an accurate and general theoretical treatment of EXAFS spectra has emerged, and the development of analysis packages such as FEFF has made the EXAFS technique a reliable method for local structure determination[46–52]. EXAFS has significant advantages for detecting doped impurities at very low atomic concentrations, thanks to its element sensitivity. In addition to the local crystal structure, the electronic structure of dilute dopants can also be studied using x-ray absorption near-edge structure (XANES).

In this paper, we report comprehensive EXAFS and XANES studies on polycrystalline Yb and Ga-containing skutterudites in order to probe the local structure and Yb, Ga site occupancy in a quantitative manner. Our EXAFS data provides direct evidence that Ga atoms in Co_4Sb_{12}-based skutterudites not only occupies the 2a void site but also replaces Sb in the 24g site. In addition, we found that as Yb filling concentration increases, the fraction of Ga replacing Sb (24g site) increases, and reaches 100% when $x = 0.4$. Our experimental results could be explained with the dual-site defect model, in which Ga in the off-center void forms a compound defect with the Ga occupying the nearby 24g site. However, Yb filler remains in the usual central 2a position regardless of doping level. These observations are also supported by the electronic structure information extracted from our XANES analysis. The implication of our findings on the solubility limit and thermoelectric properties is also discussed.

II. EXPERIMENTAL DETAILS

$Yb_xGa_{0.2}Co_4Sb_{11.933}$ (x=0.05, 0.10, 0.15, 0.20), $Yb_xGa_{0.15}Co_4Sb_{11.95}$ (x=0, 0.25, 0.30, 0.35, 0.40) and $Yb_xCo_4Sb_{12}$ (x=0.26, 0.30, 0.35, 0.40) were synthesized as described in Ref. 43, and then sintered using both hot press and spark plasma sintering methods. The sintered bulk samples were quantitatively analyzed elsewhere[43] and then ground into fine powders. Crystalline phase purity was examined by powder x-ray diffraction at room temperature using Cu Kα radiation, as shown in the Supplemental Material[53]. Rietveld refinements were performed to extract lattice constants for each sample, which

are listed in Table I. We were not able to meaningfully refine the position of Ga, as x-ray diffraction refinement is insensitive to the small amount of Ga. Ignoring Ga still allows us to obtain good fits as indicated by the small reduced-χ^2 values in the range of 1.05 to 1.6. In the current study, we label all samples as $Yb_xGa_yCo_4Sb_{12}$, where x, y represent the nominal filling fraction of Yb and Ga, respectively. Samples with $y = 0.15$ and $y = 0.2$ do not exhibit any significant difference in their physical properties, and we will not distinguish between them throughout this paper.

All x-ray absorption measurements were carried out at the Canadian Light Source (CLS) on the hard x-ray microanalysis (HXMA) beamline 06ID-1. Ga K-edge (10367 eV) data were collected for all samples and Yb L_2-edge (9978 eV) data for select samples. The energy of the incident x-ray beam was selected using a double-crystal Si(111) monochromator, with higher harmonic contributions suppressed by a 50% detuning of the second crystal. Relatively low concentrations of Yb and Ga elements make transmission geometry not suitable. All EXAFS measurements were performed in a 90° fluorescence geometry using an array of 32-element Ge solid-state detectors, with the sample 45° to the incident beam. Yb EXAFS data were collected at the L_2-edge rather than the L_3-edge because the Yb Lα fluorescence line falls on the tail of the strong Co Kβ emission line, limiting the signal-to-noise ratio for the Yb L_3 data. As a result, Yb L_2-edge data were collected using the Yb Lβ_1 fluorescence line. A standard Ta foil was utilized for in-step energy calibration. As a reference, Ta L_3-edge (9881 eV) spectra were also collected along with each Ga or Yb EXAFS measurement. Each sample was diluted with pure boron nitride powder, finely ground, pressed into a uniform pellet, and then affixed to a polyimide tape. These procedures were done in order to achieve suitable element concentration and uniformity. The Ga K-edge EXAFS data were collected with a step size of 10 eV in the pre-edge region (-200 eV to -30 eV), 0.5 eV in the near-edge region (-30 eV to 80 eV), and 0.05 Å^{-1} in the extended region (80 eV to 15 Å^{-1}). The Yb L_2-edge EXAFS data were collected with a step size of 10 eV in the region of (-200 eV to -120 eV), 0.5 eV in the Ta L_3-edge region (-120 eV to -70 eV), 5 eV in the pre-edge region (-70 eV to 30 eV), 0.5 eV in the near-edge region (-30 eV to 80 eV), and 0.05 Å^{-1} in the extended region (80 eV to 11 Å^{-1}). At each edge for each sample, in order to guarantee data reproducibility and good signal-to-noise ratio, three or more scans were collected and then averaged. All data sets were collected at room temperature.

EXAFS data obtained in energy-space were reduced using standard procedures[46]. The resulting k-space data were Fourier transformed (FT) to r-space, yielding peaks that correspond to different shells of neighboring atoms

in the EXAFS equation:

$$\chi(k) = \sum_j \frac{S_0^2 N_j e^{-2k^2\sigma_j^2} e^{-2r_j/\lambda(k)} f_j(k)}{kr_j^2} \sin(2kr_j + \delta_j(k))$$

(1)

where j represents different coordination shells made up of N_j identical atoms at approximately the same distance from the absorbing atom; S_0^2 is the amplitude reduction factor which corrects for multielectron scattering and other experimental effects (in general, $0.7 \lesssim S_0^2 \lesssim 1.2$)[54,55]; σ_j^2 is the mean-square disorder factor of the bond length r_j, including both thermal and static disorder; $f_j(k)$ and $\delta_j(k)$ are the scattering factor and scattering phase shift, which are provided in the FEFF program[46,47]; $\lambda(k)$ is the mean-free-path of the photo-electron; $k = \sqrt{2m(E - E_0)/\hbar^2}$, where E_0 is the theoretical Fermi level position. By fitting the r-space data to a sum of complex phase and amplitude functions calculated using the FEFF program, we extract bond lengths (r_j) and mean-square disorder factors (σ_j^2) for selected atom pairs, in addition to S_0^2 and $\triangle E_0$ (the shift in the edge energy from the theoretical value), for each edge. Examples of the room temperature Ga K-edge k-space data weighted with k^2 for selected compounds are shown in Fig. 1; as a comparison, low temperature data for one selected sample was also measured (See Fig. S2 in the Supplemental Material[53]). In this analysis, the FT of k-, k^2-, and k^3-weighted $\chi(k)$ were examined simultaneously and we evaluated the sum R-factor to obtain the best fit. Also, we fit both real and imaginary parts of the r-space data with the constraints described in the next section.
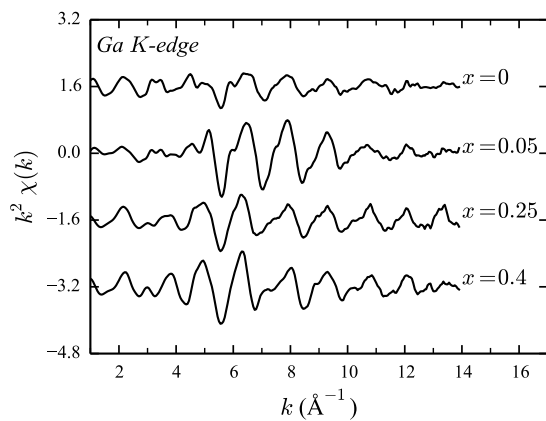

FIG. 1. Examples of Ga K-edge k-space EXAFS data collected at room temperature for $Yb_xGa_{0.15}Co_4Sb_{12}$ ($x = 0, 0.05, 0.25, 0.4$) samples, showing the good quality of the data.

III. RESULTS AND ANALYSIS

A. Local structure of Ga

Figure 2 shows the Ga K-edge r-space data for $Yb_xGa_yCo_4Sb_{12}$ ($y = 0.15$ or 0.2) compounds of which Yb filling fraction gradually increases from $x = 0$ to $x = 0.4$. The main peak around 2.2 Å and the shoulder features extending to 2.85 Å contain key information regarding the local structure of Ga. The data clearly shows that Ga atoms occupy both $2a$ (atomic coordinate $(0, 0, 0)$) and $24g$ (atomic coordinate $(0, 0.335, 0.158)$) crystallographic sites. A Ga atom in a $2a$ site fills the cage void, while a Ga in a $24g$ site replaces an Sb atom, as shown in Fig. 3(a) and (b), respectively. To illustrate various path contributions to the r-space EXAFS signal shown in Fig. 2, we take $x = 0.15$ and $x = 0.35$ as two examples. The EXAFS contributions due to various single scattering paths at Ga K-edge are shown in Fig. 4.

It is worth mentioning that the Ga K-edge data for these nine samples show little evidence of any Ga occupying the Co $8c$ site (atomic coordinate $(0.25, 0.25, 0.25)$). In the Supplemental Material[53], we show in Fig. S4 that a mixture model including the Ga_{8c} could not fit the data satisfactorily. We have also collected the Co K-edge EXAFS data (See Supplemental Material[53] Fig. S5) for select samples, which shows that Ga does not replace Co, in agreement with the calculation results[42].

If Ga occupies only the $2a$ site (Fig. 3(a)), the first neighboring shell would be Ga_{2a}-Sb with a bond length of about 3.35 Å and the calculated peak position would be ≈ 3.2 Å as shown in Fig. 4 (red solid line). However, we find the first peak position around 2.2 Å for all samples as plotted in Fig. 2. One might argue that Ga still occupies a void site, but shifts to an off-centred position, which results in reduced Ga_{2a}-Sb bond length. In that case, however, we expect the EXAFS signal resulting from the Ga-Sb single path to exhibit a low-r shoulder, due to the shell structure of the heavy Sb atom, as displayed in Fig. 4 (brown solid line).(Usually the non-linearity of the phase shifts from high-Z atoms leads to multiple local maxima in the magnitude of the FT)[56]. The observed lineshape of the first peak is smooth and almost symmetric, ruling out the possibility that Ga only occupies the off-centred void site. On the other hand, if we assume that Ga occupies the Sb substitutional ($24g$) site (Fig. 3(b)), the calculated first neighboring shell Ga_{24g}-Co (≈ 2.53 Å) approximately corresponds to the first observed peak position around 2.2 Å. We therefore applied the Ga_{24g} model to fit all Ga K-edge r-space data sets using the first two atomic shells [Ga_{24g}-Co and Ga_{24g}-Sb]. However, these fits were not satisfactory either. For $x = 0$ to $x = 0.35$ fits, we found either unreasonably large values of S_0^2 or negative disorder factors σ^2 for the first shell [Ga_{24g}-Co]. Thus, Ga_{24g} cannot be the complete structure model and additional atomic shells are required in order to fit the first sets of peaks in the r-space data.
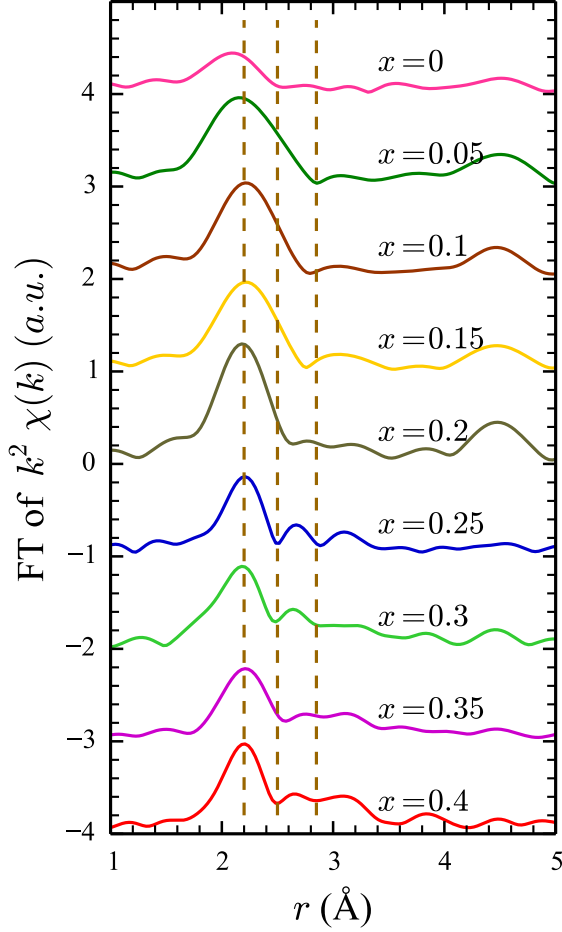
FIG. 2. (Color online) Ga K-edge data in r-space for $Yb_xGa_{0.2}Co_4Sb_{12}$ (x=0.05, 0.10, 0.15, 0.20) and $Yb_xGa_{0.15}Co_4Sb_{12}$ (x=0, 0.25, 0.30, 0.35, 0.40) compounds. Vertical dark yellow dashed lines are guides to the eye for the similarities and differences between these compounds. The FT ranges are $3 - 13.5$ Å^{-1}. Only magnitudes of the FT of $k^2\chi(k)$ are shown in this figure and the real parts can be found in the Supplemental Material[53].

Furthermore, the variations of r-space data among different Yb filling fraction samples suggest that the real local structure of Ga could be more complicated, as has been proposed by earlier theoretical works in Refs. 41 and 42.

In our dual-site model shown in Fig. 3(c), we assume that a combination of the two sites, Ga_{24g} and Ga_{2a}, exist in such a system. We also allow that the $2a$ site Ga atoms can be displaced to an off-center position due to the small atomic size of Ga and the relatively large void cage of the Co_4Sb_{12} framework, as suggested by the STEM study[43]. We introduce an off-center displacement parameter D for Ga_{2a} and choose $(D, D, 0)$ as the simplest displacement vector that can give a unique nearest-neighboring path.

A similar $(D, D, 0)$ model was also used in earlier EXAFS studies on clathrates[57,58] and skutterudites[51]. In addition, in order to allow variation in the fractional occupation of Ga_{24g} and Ga_{2a} sites, we introduce a free parameter η to represent Ga_{24g} site fractional occupancy. Then Ga_{2a} site occupancy is $(1 - \eta)$. Since η multiplies with the amplitude parameter S_0^2, these two parameters are correlated in our fitting. However, we noticed that the $x = 0.4$ data are best fitted with $S_0^2\eta = 0.99 \pm 0.05$ and $S_0^2(1 - \eta) = 0$, which indicates that for the $x = 0.4$ sample, all Ga atoms occupy the 24g sites ($\eta = 1$). Usually the S_0^2 value should not significantly vary for small concentration changes, so we decided to fix S_0^2 to 1.0 for all samples.

To fit the first peak around 2.2 Å in r-space, we considered three possible nearest-neighbor bonds: Ga_{24g}-Co, Ga_{2a}-Sb or Ga_{2a}-Ga_{24g}. However, such a short Ga-Sb bond is unphysical, suggesting that the off-centered Ga_{2a} should shift towards Ga_{24g} rather than Sb in the host network. Therefore, we used two shortest paths, Ga_{24g}-Co and Ga_{2a}-Ga_{24g} (See Fig. 3(c)), to account for the first peak. The whole EXAFS fitting equation becomes:

$$\chi = \eta\{2[Ga_{24g} - Co] + [Ga_{24g} - Sb] + ...\}$$
$$+ (1 - \eta)\{N_1[Ga_{2a} - Sb]_D + N_2[Ga_{2a} - Co]_D + ...\}$$
$$+ \min(\eta, (1 - \eta))\{2[Ga_{2a} - Ga_{24g}]_D\}$$

where the [ ] represents the contribution from the path; the first term contains the paths generated from the Ga_{24g} site, multiplied by their corresponding coordination numbers; the second term includes the paths arising from the off-centered Ga_{2a} site, with N_1 and N_2 representing the coordination numbers (7 different Ga_{2a}-Sb paths with coordination number in the ratios of 2:1:2:2:1:2:1, and 3 different Ga_{2a}-Co paths in the ratios of 2:4:2, as calculated in Ref. 51); the final term represents the Ga_{2a}-Ga_{24g} path and its fraction depends on the smaller value of η and $(1 - \eta)$; and the subscript D denotes that the free parameter D is included in the bond length[53]. We also note that an additional term $(1 - 2\eta)[Ga_{2a}$-$Sb_{24g}]$ should be present in the equation when η is less than 50% (See comments on the $x = 0$ sample in Section IV).

B. Ga dual-site results

Using the dual-site model described in the previous section, we fit Ga K-edge r-space data for samples from $x = 0$ to $x = 0.4$ in a systematic manner. Examples of r-space data and fits are plotted in Fig. 5, illustrating the good quality of the fits. All data sets are well fitted in a wide r range from 1 to 5 Å, with $x = 0.4$ resulting in a pure Ga_{24g} defect. In these fits, we included 10 paths from the Ga_{24g} absorber, 2 paths from the Ga_{2a} absorber, and one Ga_{2a}-Ga_{24g} path and thus 17 fitting parameters (13 σ^2s, one D, one η, one $\triangle E_0$ and one overall distance), still well below the number of independent points, 27, calculated using Stern's criteria[59].
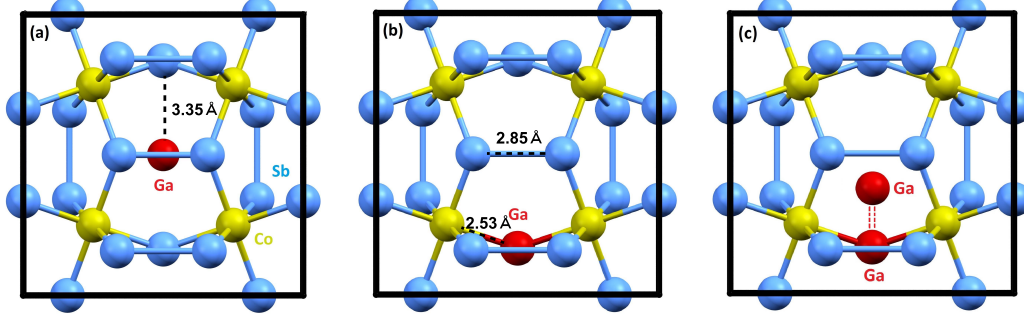
FIG. 3. (Color online) Schematic representation of the cubic crystal structure of Ga-doped Co_4Sb_{12} projected into the a-c plane, with Ga defect atoms shown in red: (a) on-center void filling Ga_{2a}; (b) Sb substitutional Ga_{24g}; (c) dual-site complex defect of Ga_{24g}-Ga_{2a}, with Ga_{2a} off-centred in the (D, D, 0) direction.

TABLE I. Lattice constants and Ga K-edge fitted parameters (r and σ^2 for Ga_{24g}-Co and Ga_{2a}-Ga_{24g} bond, respectively; Ga_{2a} off-center displacement parameter D, and Ga_{24g} site fractional occupancy η) for $Yb_xGa_yCo_4Sb_{12}$. The error bars for the lattice constants are ± 0.0003 Å. The error bars for $\sigma^2(Ga_{24g}$-Co) and $\sigma^2(Ga_{24g}$-$Ga_{2a})$ are within ± 0.0016 (Å^2) and ± 0.0030 (Å^2), respectively. In the initial fittings for all nine samples, σ^2s corresponding to the common paths are constrained to be the same, and then released to vary individually to obtain the best fit for each sample.

Compound	Lattice constant(Å)	Ga_{24g}-Co		Ga_{2a}-Ga_{24g}		D (Å)	η
		r (Å)	$\sigma^2(Å^2)$	$r(Å)$	$\sigma^2(Å^2)$		
$x = 0$	9.0390	2.48(2)	0.0057	2.35(3)	0.0080	0.77(2)	0.31±0.10
$x = 0.05$	9.0410	2.47(2)	0.0057	2.64(4)	0.0103	0.55(3)	0.49±0.06
$x = 0.10$	9.0432	2.48(1)	0.0054	2.68(3)	0.0135	0.51(2)	0.67±0.04
$x = 0.15$	9.0461	2.46(1)	0.0057	2.67(3)	0.0120	0.53(2)	0.52±0.02
$x = 0.20$	9.0491	2.47(3)	0.0051	2.64(6)	0.0110	0.55(5)	0.72±0.15
$x = 0.25$	9.0521	2.51(2)	0.0067	2.44(5)	0.0119	0.70(4)	0.57±0.05
$x = 0.30$	9.0522	2.50(1)	0.0062	2.44(5)	0.0099	0.73(4)	0.78±0.10
$x = 0.35$	9.0551	2.50(1)	0.0067	2.41(3)	0.0103	0.73(2)	0.78±0.05
$x = 0.40$	9.0590	2.50(1)	0.0067	$--$	$--$	$--$	1.0

The fitting parameters are listed in Table I. Here, as expected, the bond length of Ga_{24g}-Co is similar to that of the nearest Sb-Co distance in Co_4Sb_{12}. If Ga_{2a} is on the void center, we expect a nearest Ga_{2a}-Ga_{24g} distance to be about 3.35 Å. However, we found that Ga_{2a}-Ga_{24g} has much shorter bond distance. Our observation suggests that Ga_{2a} significantly shifts away from the void center and moves toward neighboring Ga_{24g}, leading to a severe cage distortion and a much shorter Ga_{2a}-Ga_{24g} bond length compared to those between Ga_{2a} and the other Sb atoms. This observation is consistent with recent STEM result, in which distorted skutterudite cages were observed[43]. Theoretical calculations also indicate that Ga_{2a} and Ga_{24g} are prone to attract each other and form short bonding due to the intra-defect interaction[42,44]. However, it is to be noted that the Ga-Ga bond length varies in the range of 2.3 to 2.7 Å among these nine samples because of the various D values. The difference in D explains the prominent peak around 4.5 Å for the $Yb_xGa_{0.2}Co_4Sb_{12}$ samples, which becomes much broader for the $Yb_xGa_{0.15}Co_4Sb_{12}$ as shown in Fig. 2.

One possible reason for this difference will be discussed in Section IV.

Figure 6 plots the fit results (red solid circles) of the Ga_{24g} site fraction (η) as a function of Yb filling x. The vertical error bars in Fig. 6 represent the standard deviation of the results obtained from the fitting. To estimate the uncertainty due to the data reduction procedure we repeated the analysis varying some of the most relevant parameters, for example, shortening the k range of the FT or the r fitting range, and using a single k^n weight (n=1,2 and 3); we found this uncertainty is much smaller than the standard deviation as plotted in Fig. 6. As Yb concentration increases from $x = 0.05$ to $x = 0.4$, the ratio between Ga_{24g} and Ga_{2a} increases gradually from 1:1 to 1:0. This result suggests that as the more Yb atoms fill the voids, Ga atoms are pushed from $2a$ to $24g$ sites. When the Yb concentration reaches $x = 0.4$, all doped Ga atoms have been driven to replace Sb. Our results provide quantitative experimental evidence for the variation of Ga dual-site occupancy behavior in response to the presence of the secondary fillers.
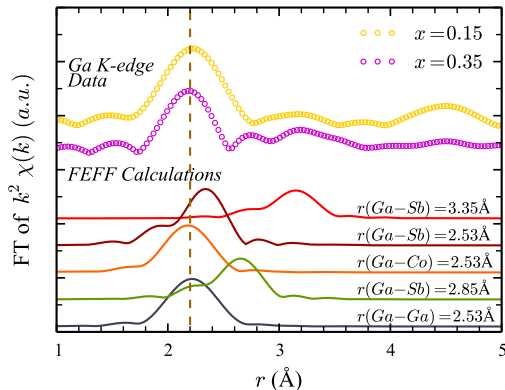
FIG. 4. (Color online) Comparison between Ga K-edge data (unfilled circles) on representative compounds and FEFF calculations (solid lines) of individual single scattering paths displayed in r-space.

C. Local structure of Yb

In order to highlight the unusual behavior of Ga fillers, we also obtained the Yb local structure using EXAFS. In Fig. 7(a) we show representative EXAFS data sets in r-space at the Yb L$_2$-edge for a selection of Yb, Ga double-doped and Yb single-doped skutterudite samples. The first peak at ≈ 3.2 Å with a shoulder around 2.4 Å is due to a Yb-Sb atom pair, for which Yb is assumed to be at the center of the cage void (2a site). A comparison of the r-space and k-space data for all compounds show very little variation of the lineshape and amplitude as a function of doping. This indicates that for all the samples studied, there is little cage distortion or bond variation in the first coordination shell (Yb$_{2a}$-Sb) as well as in the second coordination shell (Yb$_{2a}$-Co). To further investigate the local structure of Yb atoms, we have carried out fits of the EXAFS r-space data to a sum of FEFF functions for the first three single scattering shells and two multiple scattering shells. The fit range in r-space is $2-6$ Å. One constraint introduced in these fits is that we only allow bond lengths to undergo isotropic expansion/contraction, which is reasonable for a cubic lattice that does not show any phase transition. One example of these fits is shown in Fig. 7(b), including the individual EXAFS contributions from the first and second coordination shells. In these fits, we only varied 7 parameters (five σ^2s, one overall distance and one $\triangle E_0$). The fitted bond lengths of Yb$_{2a}$-Sb agree well with the diffraction result within 0.1 Å, and the corresponding mean-square disorder factors are within 0.016 Å$^2 < \sigma^2 < 0.019$ Å^2. Details of each fitting parameter can be found in the Supplemental Material[53]. No off-centering of Yb position is found. We found neither filling fraction dependence for Yb local structure, nor any effect of Ga addition on the Yb local structure.

D. XANES spectra

We display in Fig. 8(a) the near-edge absorption spectra at the Ga K-edge. In order to calibrate any possible energy drifts caused by the monochromator, Ta reference spectra were aligned carefully for all Ga K-edge measurements. The XANES data shows that the edge energy shifts slightly toward lower energy with increasing Yb filling. The shift can be observed more clearly in the second derivative shown in Fig. 8(b). The second derivative peak of the $x = 0.4$ sample near $E - E_0 = 0$ is located at lower energy than the one for $x = 0.05$ samples. Also prominent in the second derivative comparison is the well-defined negative peak just above the edge in the $x = 0.05$ sample (called 'post-edge' peak), which becomes weaker and broader in the $x = 0.4$ sample. To model the observed XANES result, we note that Ga on 2a or 24g site have different valence states and are expected to produce very different XANES spectra. Therefore, it is reasonable to expect that the observed XANES spectra would be reproduced by a linear combination of the XANES spectrum from each site. We simulated the XANES spectra with the FEFF program[47], which uses the muffin-tin approximation to obtain the monoelectronic potentials. Real-space atomic clusters based on two kinds of crystallographic sites (2a and 24g) in Co$_4$Sb$_{12}$ were constructed and used throughout the calculations. The cluster sizes were chosen to cover one unit cell. Several atomic configurations were tested and the most stable configuration obtained from our EXAFS results was adopted. Finally, a linear combination was performed by carefully adding up the calculated 2a site- and 24g site- Ga K-edge XANES spectra with different ratios.

Figure 8(c) shows the linear combination results of the calculated XANES spectra. The overall trend observed in our XANES experiment is reasonably reproduced by the simulated XANES spectra. Note that our EXAFS data suggests that the Ga$_{24g}$:Ga$_{2a}$ ratio for $x = 0.05$ is about 1:1 (the third simulated spectrum from the top in Fig. 8(c)); the 0:1 and 0.5:1 simulations are plotted as reference. The second derivatives of the calculated XANES for Ga$_{24g}$:Ga$_{2a}$=1:1 and Ga$_{24g}$ only configurations are plotted in Fig. 8(d), showing the small edge shift between the 2a and the 24g site. Also apparent is the post-edge peak for the Ga$_{24g}$:Ga$_{2a}$=1:1 mixing configuration. Therefore, one can conclude that this post-edge peak is a tell-tale signature of the Ga$_{2a}$ site, which disappears for $x = 0.4$ sample, as expected from our EXAFS results. The XANES calculation also captures the shift of the absorption edge to lower energy as the Ga$_{24g}$ fraction increases. This observation is consistent with the picture proposed in the charge-compensated compound defect model[41], in which the Ga$_{2a}$ is in the higher valence state than that of the Ga$_{24g}$, since the absorption edge tends to shift to lower energy for lower valence ions. Overall, the doping dependence of the XANES spectra also indicates that the fraction of Ga$_{24g}$ in Yb$_x$Ga$_{0.2}$Co$_4$Sb$_{12}$ increases
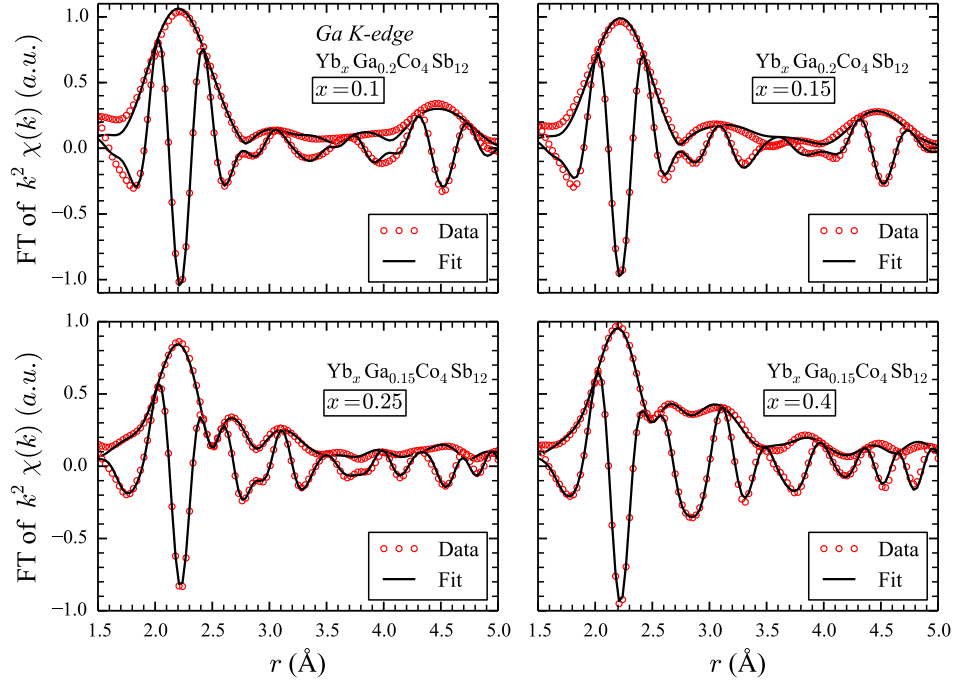
FIG. 5. (Color online) Ga K-edge data for $Yb_xGa_yCo_4Sb_{12}$ in r-space and the fit results based on the dual-site defects model. The fit ranges are $1-5$ Å. The high frequency curve below the envelop is the real part of the Fourier transform (FT_R). The envelope is the magnitude of the Fourier transform, defined as $\sqrt{FT_R^2 + FT_I^2}$, where FT_I (not shown) is the imaginary part of the Fourier transform.
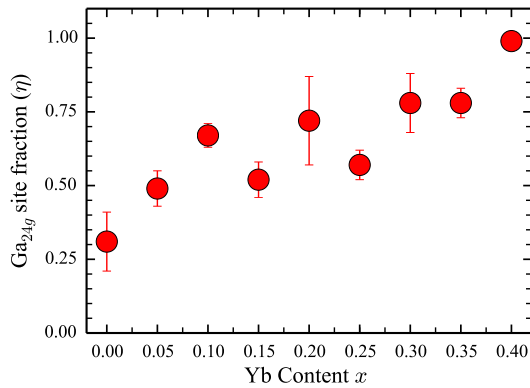

FIG. 6. (Color online) Yb content (x) dependent Ga_{24g} site fractions (η) obtained from fits for Ga K-edge data in r-space. The corresponding Ga_{2a} site fractions are ($1 - \eta$).

with increasing Yb concentration.

It is worth mentioning that no energy shift is observed at the Yb L_2-edge, which suggests that the Yb dopant has the same valence state regardless of the filling fraction.

IV. DISCUSSION AND CONCLUSIONS

Our EXAFS study provides direct observation of the Ga atoms occupying both the $24g$ and the $2a$ sites in the Co_4Sb_{12}-based skutterudites, of which the distinct two sites of Ga were difficult to confirm in previous experimental studies. Such observation explains the unusual transport properties of Ga-doped skutterudite materials, as compared to normal alkaline- or rare-earth filled skutterudites[11,38,41].

In order to understand the physical origin of the gradually increasing Ga_{24g} site occupancy with Yb concentration as shown in Fig. 6, it is useful to consider the charge-compensated compound defect (CCCD) model for Ga-doped Co_4Sb_{12}[41]. In particular, in their theoretical work using ab initio total-energy calculations[42], Xi and coworkers found that the dominant defect in Ga doped Co-Sb skutterudite is the complex dual-site occupancy defect with the Ga_{24g}:Ga_{2a} ratio of 1:2. However, at high carrier concentrations with significant Fermi level shifts (~ 0.2 eV), the Ga_{24g} only defect has a charge state of -2 and becomes more stable than any other defects. Our x-ray absorption data qualitatively agree with this theoretical prediction. We find that the ratio between Ga_{24g} and Ga_{2a} is about $1:1$ when there is a small amount of Yb fillers ($x = 0.05$) and the ratio becomes $1:0$ when
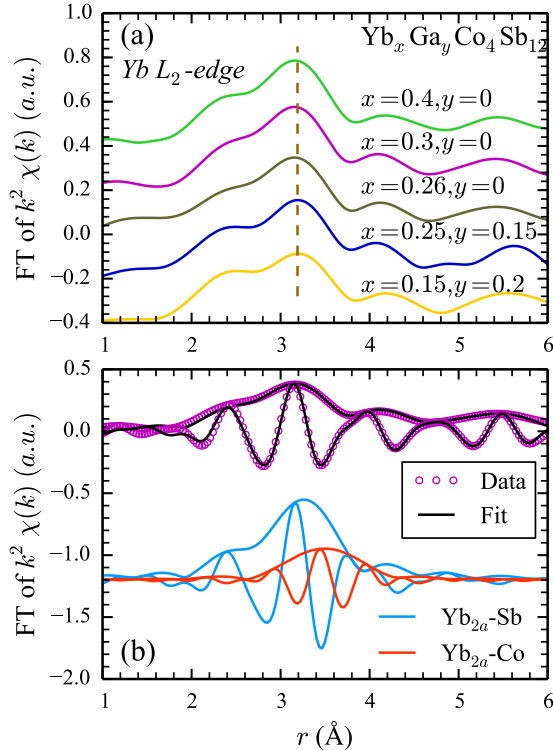
FIG. 7. (Color online) (a) Plots of the r-space data for the Yb L_2-edge. There is no significant Yb filling fraction dependence or Ga-added effects. The expected positions of the first neighbors are indicated by vertical dark yellow dashed lines. The FT ranges are $3 - 9$ Å^{-1} for each sample. (b) Fit to the r-space data for $Yb_{0.3}Co_4Sb_{12}$ and peaks from Yb_{2a}-Sb and Yb_{2a}-Co coordination shells. The fit range is $2 - 6$ Å.

the Yb filling concentration increases to $x = 0.4$. Since Yb acts as an electron donor, increased Yb concentration seems to have the effect of shifting the Fermi level to higher energy. In other words, as a secondary void filler, Yb competes with Ga_{2a} thermodynamically and drives Ga_{2a} defects into Ga_{24g} defects at higher concentrations of Yb. Our experimental results show this both structurally through EXAFS and electronically through XANES. One interesting future direction is to examine the role of In dopants. Despite the fact that both In and Ga are group 13 dopants, Xi et al. found that they behave somewhat differently in Co_4Sb_{12} host structure[42].

Our observations provide an explanation for an important question about Yb solubility in Co_4Sb_{12} skutterudites. The filling fraction of Yb (up to 0.4 on the $2a$ sites) in Ga,Yb co-doped samples is much higher than the solubility limit of Yb single-doped samples, which was previously determined to be around 0.22[26]. This can be understood by the fact that the introduction of electron deficient Ga_{24g} boosts the compound's capability to accommodate more electron donors. A careful examination

of the local structure gives further credence to this picture. Like most rare-earth filler species, Yb expands the skutterudite cage lattice slightly, whereas adding Ga decreases the lattice constants compared to Yb single filled Co_4Sb_{12}. Detailed investigation of the lattice constants can be found in the x-ray powder diffraction results of Ref. 43. As shown in the EXAFS fit results in Table I, the fitted nearest-neighbor [Ga_{24g}-Co] bond lengths are $2.46 - 2.50$ Å which is slightly shorter than the bond length between Sb and Co in unfilled Co_4Sb_{12} structure (≈ 2.53 Å). This means that the presence of Ga_{24g} is most likely causing the observed lattice contraction in Ga filled Co_4Sb_{12}. The lattice expansion due to Yb filler atoms and the contraction due to Ga atoms compensate for each other, so that more Yb atoms can enter the cages as more Ga atoms occupy the Sb substitutional site.

Another important observation from our study is the contrast between Yb and Ga dopants even when the Ga atoms fill the cage voids. Our Yb EXAFS data can be consistently described by the structure with Yb at the center of the cage void, without any indication of off-center displacement. On the other hand, our fits to the Ga EXAFS data consistently give the displacement parameter (D) of 0.5-0.8 Å (Table I), indicating that the Ga_{2a} dopants are significantly displaced from the void center. The D values obtained for the $Yb_xGa_{0.2}Co_4Sb_{12}$ samples are relatively smaller than those for $Yb_xGa_{0.15}Co_4Sb_{12}$ samples. So far, we do not have a good understanding of the cause of this difference, since the samples are synthesized in exactly the same manner and other physical properties are almost identical according to previous investigation of these samples by some of the coauthors[43]. We, however, think that the variation in D might indicate that Ga_{2a}-Ga_{24g} does not form a covalent bond entirely, and there is some ionic tendency between them. This is consistent with the observation in other materials that various Ga-Ga pair distances were reported in a single structure[60,61].

It should be emphasized that the local structure of Ga determined by our EXAFS is consistent with other supporting room temperature studies, such as diffraction anomalous near-edge structure (DANES) measurements. As illustrated in the Supplemental Material[53], our preliminary DANES data shows clear contrast between the $x = 0$ and $x = 0.4$ samples, providing direct evidence that the site occupancy behaviors of Ga in these two compounds are distinctly different. Similar contrast has also been revealed by the calculated DANES assuming that Ga occupies the $2a$ or $24g$ site exclusively. These results complement our EXAFS and XANES data and bring home the message that there are two distinct Ga sites in the samples we studied.

Lastly, we would like to comment on the $x = 0$ sample. The dual-site model (Fig. 3(c)) we used requires that each Ga_{2a} displaces from the on-center void position and moves toward the neighboring Ga_{24g}. However, in particular for the $x = 0$ sample, our EXAFS data indicates that the Ga_{24g} site fraction is less than 50% and
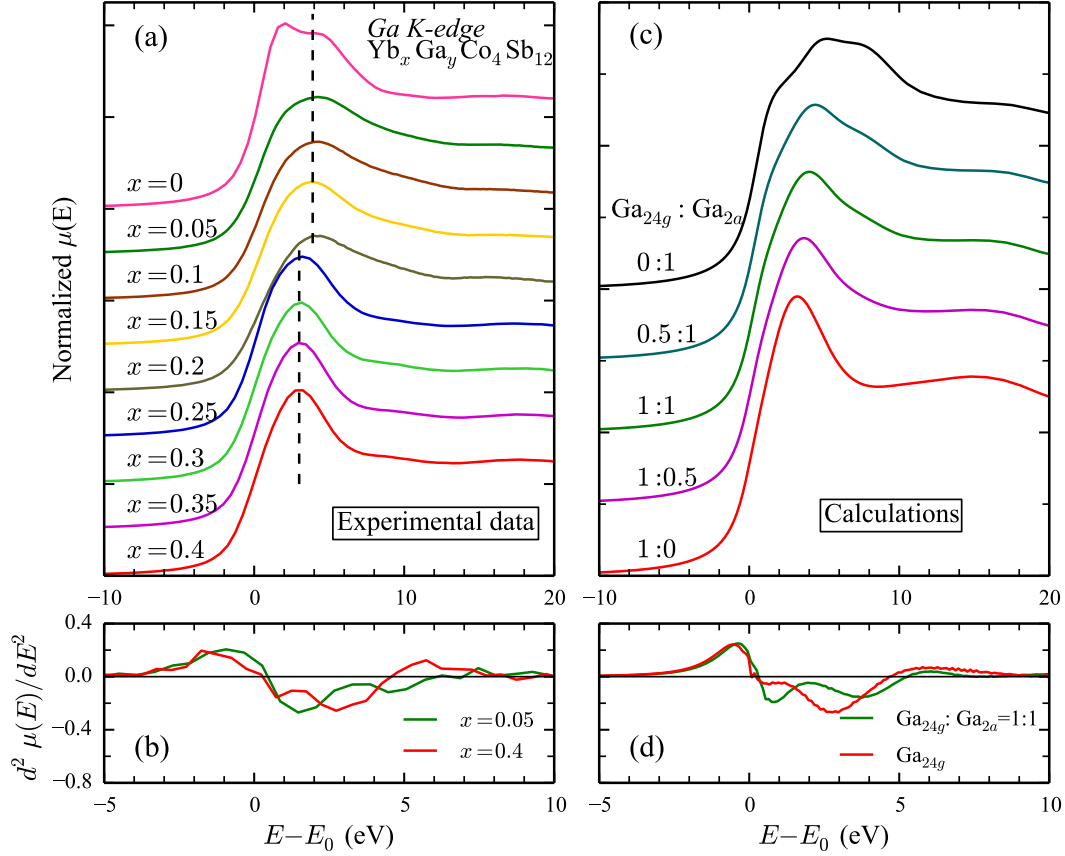
FIG. 8. (Color online) (a) Ga K-edge XANES spectra for $Yb_xGa_yCo_4Sb_{12}$ compounds ($x = 0$ to 0.4, from top to bottom) obtained from experiments. Vertical black dashed lines are displayed as guides to the eye. $E_0 = 10371$ eV is determined from the experimental data of $x = 0.4$ (energy at the half-height position on the edge). (b) The second derivative spectra of the experimental XANES of $x = 0.05$ and $x = 0.4$. (c) Calculated Ga K-edge XANES spectra for complex Ga_{24g}-Ga_{2a} structure with varied dual-site ratios listed in the figure. (d) The second derivative spectra of the calculated XANES for Ga_{24g}:$Ga_{2a} =$ 1:1 and Ga_{24g} single defect structures.

that there are still a small fraction of Ga_{2a} atoms that do not have neighboring Ga_{24g}. Although the r-space data can be reasonably fitted without incorporating this small fraction of Ga_{2a} into the EXAFS equation, we suspect that this fitting might not be unique and that it is rather difficult to interpret the local structure of Ga on multiple possible sites, given the complexity of this particular $x = 0$ sample. We showed the EXAFS, XANES and DANES results for the $x = 0$ sample to provide a comparison with those samples with both Ga and Yb doping. Full understanding of the defect model in this case will probably require other measurements with higher precision.

In summary, we present a comprehensive local structure study of $Yb_xGa_yCo_4Sb_{12}$ compounds ($x = 0.05$ to 0.4). Our results confirm that the actual defect structure for Ga-doped skutterudites is quite complex; two crystallographic sites can be occupied by Ga atoms: the 24g site

replacing Sb or the 2a off-centered void site. The most important new result from this study is that the fraction of Ga occupying the 24g site increases gradually as a function of additional Yb, reaching 100 % when $x = 0.4$. This general trend can serve as an important strategy to optimize the thermoelectric performance in partially filled skutterudites. Combined with the Fermi level shift observed in the XANES spectra, we find that the charge-compensated compound defect model can explain the observed increase of Ga_{24g} fraction very well. Our study illustrates that combined near-edge and extended x-ray absorption spectroscopy is a powerful method to investigate the crystal and electronic structure of complex local defects. This method will be especially valuable for studying structural and electronic properties of dilute dopants.

---

[*] yjkim@physics.utoronto.ca

[1] G. A. Slack, in *CRC Handbook of Thermoelectrics*, edited by D. M. Rowe (CRC Press, 1995) pp. 407–440.

[2] B. C. Sales, D. Mandrus, and R. K. Williams, Science **272**, 1325 (1996).

[3] B. C. Sales, D. Mandrus, B. C. Chakoumakos, V. Keppens, and J. R. Thompson, Phys. Rev. B **56**, 15081 (1997).

[4] G. S. Nolas, M. Kaeser, R. T. Littleton, and T. M. Tritt, Appl. Phys. Lett **77**, 1855 (2000).

[5] Y. Tang, R. Hanus, S. W. Chen, and G. J. Snyder, Nat. Commun. **6**, 7584 (2015).

[6] J. P. Fleurial, A. Borshchevsky, T. Caillat, and R. Ewell, in *Energy Conversion Engineering Conference, 1997. IECEC-97., Proceedings of the 32nd Intersociety* (1997) pp. 1080–1085 vol.2.

[7] J. W. Fairbanksl, in *Vehicular Thermoelectrics: A New Green Technology in Directions in Engine-Efciency and Emission Research (DEER) Conference Presentations* (2011).

[8] G. Nolas, D. Morelli, and T. M. Tritt, Annu. Rev. Mater. Sci. **29**, 89 (1999).

[9] G. J. Snyder and E. S. Toberer, Nat. Mater. **7**, 105 (2008).

[10] M. Rull-Bravo, A. Moure, J. F. Fernandez, and M. Martin-Gonzalez, RSC Adv. **5**, 41653 (2015).

[11] X. Shi, S. Bai, L. Xi, J. Yang, W. Zhang, L. Chen, and J. Yang, J. Mater. Res. **26**, 1745 (2011).

[12] L. D. Chen, T. Kawahara, X. F. Tang, T. Goto, T. Hirai, J. S. Dyck, W. Chen, and C. Uher, J. Appl. Phys. **90**, 1864 (2001).

[13] V. Keppens, D. Mandrus, B. C. Sales, P. Dai, R. Coldea, M. B. Maple, D. A. Gajewski, E. J. Freeman, and S. Bennington, Nature **395**, 876 (1998).

[14] E. Bauer, A. Galatanu, H. Michor, G. Hilscher, P. Rogl, P. Boulet, and H. Noël, The European Physical Journal B - Condensed Matter and Complex Systems **14**, 483 (2000).

[15] R. P. Hermann, R. Jin, W. Schweika, F. Grandjean, D. Mandrus, B. C. Sales, and G. J. Long, Phys. Rev. Lett. **90**, 135505 (2003).

[16] M. Christensen, A. B. Abrahamsen, N. B. Christensen, F. Juranyi, J. Andersen, C. R. H. Bahl, and B. B. Iversen, Nat. Mater. **7**, 811 (2008).

[17] I. K. Dimitrov, M. E. Manley, S. M. Shapiro, J. Yang, W. Zhang, L. D. Chen, Q. Jie, G. Ehlers, A. Podlesnyak, J. Camacho, and Q. Li, Phys. Rev. B **82**, 174301 (2010).

[18] J. L. Feldman, D. J. Singh, I. I. Mazin, D. Mandrus, and B. C. Sales, Phys. Rev. B **61**, R9209 (2000).

[19] M. M. Koza, M. R. Johnson, R. Viennois, H. Mutka, L. Girard, and D. Ravot, Nat. Mater. **7**, 805 (2008).

[20] P. Ghosez and M. Veithen, J. Phys.: Condens. Matter **19**, 096002 (2007).

[21] G. S. Nolas, J. L. Cohn, and G. A. Slack, Phys. Rev. B **58**, 164 (1998).

[22] D. T. Morelli, G. P. Meisner, B. Chen, S. Hu, and C. Uher, Phys. Rev. B **56**, 7376 (1997).

[23] G. A. Lamberton, S. Bhattacharya, R. T. Littleton, M. A. Kaeser, R. H. Tedstrom, T. M. Tritt, J. Yang, and G. S. Nolas, Appl. Phys. Lett **80**, 598 (2002).

[24] V. L. Kuznetsov, L. A. Kuznetsova, and D. M. Rowe, J. Phys.: Condens. Matter **15**, 5035 (2003).

[25] M. Puyet, B. Lenoir, A. Dauscher, M. Dehmas, C. Stiewe, and E. Mller, J. Appl. Phys. **95**, 4852 (2004).

[26] X. Shi, W. Zhang, L. D. Chen, and J. Yang, Phys. Rev. Lett. **95**, 185503 (2005).

[27] Z. G. Mei, W. Zhang, L. D. Chen, and J. Yang, Phys. Rev. B **74**, 153202 (2006).

[28] Y. Z. Pei, L. D. Chen, W. Zhang, X. Shi, S. Q. Bai, X. Y. Zhao, Z. G. Mei, and X. Y. Li, Appl. Phys. Lett. **89**, 221107 (2006).

[29] L. Xi, J. Yang, W. Zhang, L. Chen, and J. Yang, J. Am. Chem. Soc. **131**, 5560 (2009).

[30] W. Zhao, P. Wei, Q. Zhang, C. Dong, L. Liu, and X. Tang, J. Am. Chem. Soc. **131**, 3713 (2009).

[31] L. Zhang, A. Grytsiv, P. Rogl, E. Bauer, and M. Zehetbauer, J. Phys. D: Appl. Phys. **42**, 225405 (2009).

[32] J. R. Salvador, J. Yang, H. Wang, and X. Shi, J. Appl. Phys. **107**, 043705 (2010).

[33] X. Shi, J. Yang, J. R. Salvador, M. Chi, J. Y. Cho, H. Wang, S. Bai, J. Yang, W. Zhang, and L. Chen, J. Am. Chem. Soc. **133**, 7837 (2011).

[34] J. Peng, W. Xu, Y. Yan, J. Yang, L. Fu, H. Kang, and J. He, J. Appl. Phys. **112**, 024909 (2012).

[35] N. R. Dilley, E. D. Bauer, M. B. Maple, and B. C. Sales, J. Appl. Phys. **88**, 1948 (2000).

[36] T. He, J. Chen, H. D. Rosenfeld, and M. A. Subramanian, Chem. Mater. **18**, 759 (2006).

[37] R. C. Mallik, E. Mueller, and I.-H. Kim, J. Appl. Phys. **111**, 023708 (2012).

[38] W. Zhao, P. Wei, Q. Zhang, H. Peng, W. Zhu, D. Tang, J. Yu, H. Zhou, Z. Liu, X. Mu, D. He, J. Li, C. Wang, X. Tang, and J. Yang, Nat. Commun. **6**, 7197 (2015).

[39] A. Harnwunggmoung, K. Kurosaki, T. Plirdpring, T. Sugahara, Y. Ohishi, H. Muta, and S. Yamanaka, J. Appl. Phys. **110**, 013521 (2011).

[40] H. Li, X. Tang, Q. Zhang, and C. Uher, Appl. Phys. Lett. **94**, 102114 (2009).

[41] Y. Qiu, L. Xi, X. Shi, P. Qiu, W. Zhang, L. Chen, J. R. Salvador, J. Y. Cho, J. Yang, Y.-C. Chien, S.-W. Chen, Y. Tang, and G. J. Snyder, Adv. Funct. Mater. **23**, 3194 (2013).

[42] L. Xi, Y. Qiu, S. Zheng, X. Shi, J. Yang, L. Chen, D. J. Singh, J. Yang, and W. Zhang, Acta Mater. **85**, 112 (2015).

[43] X. Shi, J. Yang, L. Wu, J. R. Salvador, C. Zhang, W. L. Villaire, D. Haddad, J. Yang, Y. Zhu, and Q. Li, Sci. Rep. **5**, 14641 (2015).

[44] Y. Qiu, J. Xing, X. Gao, L. Xi, X. Shi, H. Gu, and L. Chen, J. Mater. Chem. A **2**, 10952 (2014).

[45] Y. Tang, Y. Qiu, L. Xi, X. Shi, W. Zhang, L. Chen, S.-M. Tseng, S.-W. Chen, and G. J. Snyder, Energy Environ. Sci. **7**, 812 (2014).

[46] B. Ravel and M. Newville, J. Synchrotron Radiat. **12**, 537 (2005).

[47] J. J. Rehr, J. J. Kas, F. D. Vila, M. P. Prange, and K. Jorissen, Phys. Chem. Chem. Phys. **12**, 5503 (2010).

[48] D. Cao, F. Bridges, P. Chesler, S. Bushart, E. D. Bauer, and M. B. Maple, Phys. Rev. B **70**, 094109 (2004).

[49] F. Bridges, Mod. Phys. Lett. B **30**, 1630001 (2016).

[50] M. Short, F. Bridges, T. Keiber, G. Rogl, and P. Rogl, Intermetallics **63**, 80 (2015).

[51] T. Keiber, F. Bridges, R. E. Baumbach, and M. B. Maple, Phys. Rev. B **86**, 174106 (2012).

[52] T. Keiber, F. Bridges, and B. C. Sales, Phys. Rev. Lett. **111**, 095504 (2013).

[53] Supplemental Material.

[54] J. J. Rehr, E. A. Stern, R. L. Martin, and E. R. Davidson, Phys. Rev. B **17**, 560 (1978).

[55] B. K. Teo, *Extended X-ray Absorption Fine Structure (EXAFS) Spectroscopy* (Springer, 1986).

[56] G. G. Li, F. Bridges, and C. H. Booth, Phys. Rev. B **52**, 6332 (1995).

[57] R. Baumbach, F. Bridges, L. Downward, D. Cao, P. Chesler, and B. Sales, Phys. Rev. B **71**, 024202 (2005).

[58] Y. Jiang, F. Bridges, M. A. Avila, T. Takabatake, J. Guzman, and G. Kurczveil, Phys. Rev. B **78**, 014111 (2008).

[59] E. A. Stern, Phys. Rev. B **48**, 9825 (1993).

[60] M. Bernasconi, G. L. Chiarotti, and E. Tosatti, Phys. Rev. B **52**, 9988 (1995).

[61] S.-M. Park, S.-J. Kim, and M. G. Kanatzidis, J. Solid State Chem. **177**, 2867 (2004).